Energy Conversion and Management 171 (2018) 1083–1092

Contents lists available at ScienceDirect

Energy Conversion and Management

journal homepage: www.elsevier.com/locate/enconman

In situ synthesized electroactive and large dielectric BaF_2/PVDF nanocomposite film for superior and highly durable self-charged hybrid photo-power cell

Farha Khatun[a], Pradip Thakur[b,*], Nur Amin Hoque[a], Arpan Kool[a], Swagata Roy[a], Prosenjit Biswas[a], Biswajoy Bagchi[c], Sukhen Das[a,*]

[a] Department of Physics, Jadavpur University, Kolkata 700032, India
[b] Department of Physics, Netaji Nagar College for Women, Kolkata 700092, India
[c] Department of Medical Physics and Biomedical Engineering, University College London, London, United Kingdom

ARTICLE INFO

Keywords:
PVDF
β phase
Dielectric
Self-charging
Power, durable

ABSTRACT

In present work, a simplistic, efficient and highly durable electroactive and high dielectric BaF_2 nanoparticles (NPs) incorporated polyvinylidene fluoride (PVDF) thin film based Self-Charged Hybrid Photo-Power Cell (HPPC) has been designed which is able to self-charge under visible light illumination. The incorporation of NPs into the PVDF matrix has effectively enhanced the polar β crystallite nucleation (~96%) and the dielectric value (~2570) of the PVDF thin film. A composite dye film of TiO_2 NPs, phenosafranine-polyvinyl pyrrolidone in the presence of H_3PO_4 is acted as the light absorbing and photoelectrons generating part in the HPPC. The photo-electrons are stored in the energy storage part made of the *in situ* synthesized BaF_2 NPs embedded PVDF thin film. Our HPPC is able to generate a photovoltage ~1.3 V within 65 s under exposure of visible light (~110 mW/cm^2) with superior energy storage efficiency ~79%. The device has the ability of storing charge ~1200 F/m^2 with power density ~18.7 W/m^2 and charge density ~1500 C/m^2. Our light weighted self-charged power bank may be utilized as power supplier in portable electronic appliances.

1. Introduction

Safety of energy, environment and economical condition are the most important issue of our entire human society in the 21st century [1]. To resolve the critical problem of overall energy demands in a sustainable fashion, it is very essential to replace the traditional fossil fuels (e.g. coal, petroleum, gas etc.) by the naturally available renewable energy sources (like sunlight, wind, water, biomass energies, geothermal and mechanical resources) in our living system because of their rapid demolition and related environmental pollution and global warming issues [2,3]. The basic strength of the modern social activities have been resolved around the conversion of the electrical energy from living systems and the storage of the energy with enhanced power quality [4,5]. Thus, the researchers and engineers are highly involved to develop advance multifunctional materials and techniques for the conversion of other form of energies like solar energy and mechanical energy to electrical energy. Conversion of solar energy to electrical energy is highly appreciated from the beginning by renewable energy researchers due to unlimited supply of eco-friendly sunlight and their large scale application possibilities in our society [6,7].

Recently, piezoelectric nanogenerators (PENGs), dye-sensitized solar cells and perovskite solar cells are some popular techniques of energy conversion from mechanical and solar energy respectively [7,9]. Self-charging hybrid power cell capable for both energy generation and storage is a new and promising approach in renewable energy fields [10–12]. Integration of solar energy conversion units (i.e. dye sensitized solar cell, organic photovoltaic (OPV), perovskite solar cell etc.) with an energy storage systems (i.e. Li-ion batteries, supercapacitors etc.) have been previously reported by some researchers [8,13–24]. Integrations of energy generator and storing part have decreased the overall outputs due to increase of net resistance and limitations to rule the light illumination. These shortcomings may be defeated by integrating the energy harvesting unit and storage part in same unit. Recently, Wee at al. designed a photo-supercapacitor combining a OPV and carbon nanotube based supercapacitor with low power loss [16]. Zhang et al. reported an integrated power cell by combining a dye-sensitized solar cell energy storage function through PVDF/ZnO nanocomposites (NCs) (energy density ~ 1.4 mWh kg^{-1}) [15]. Extensive research works have

* Corresponding authors.
E-mail addresses: pradipthakurju@gmail.com (P. Thakur), sdasphysics@gmail.com (S. Das).

https://doi.org/10.1016/j.enconman.2018.06.050
Received 18 March 2018; Received in revised form 26 May 2018; Accepted 14 June 2018

been carried out to develop high dielectric polymer or polymer NCs for energy storing. The polymeric NCs with very good dielectric properties may be a promising prospects for fabricating superior self-charged hybrid photo-power cell. But, design of high dielectric polymer based efficient hybrid polymeric solar cells with energy storage capability are few till now. Piezoelectric PVDF is considerably applied for harvesting electrical energy from mechanical energy. But, the applications of PVDF in hybrid photo induced power cell are very few [24,25]. Previously we have successfully designed some high dielectric polymeric films based simplistic two electrode self-charged photo-power cells using polyvinylidene fluoride (PVDF) and their composites or NCs thin films as efficient energy reservoir in a single unit [22–24].

PVDF, with molecular structure $(–CH_2\text{-}CF_2–)_n$, is a semi-crystalline, flexible, electroactive polymer, which is exceptionally attracted by the present researchers for its superior properties i.e. dielectric, Piezo, Pyro and Ferroelectricity. PVDF is extremely applied in different fields like-sensors and memory devices, batteries, thin film transistors, PENGs, self-charging storage devices as well as in biomedical fields [24–29]. PVDF has five distinct crystalline polymorphs α, β, γ, δ and ε. Among those phases α and ε are completely non-polar and β, γ and δ are polar. Two antiparallel arrangement of the dipole moments in the monoclinic unit cell of the lattice structure form non-polar groups and establish its TGTG' (trans-gauche + -trans-gauche -) dihedral polymeric chain configuration. β phase is the most electroactive polymorph of PVDF due to the highest dipolar moment per unit cell (8×10^{-30} C m) which has raised due to the orthorhombic unit cell matrix and *all trans* i.e. TTTT planar zigzag conformation [26,30,31]

In present study, the electroactive β phase rich and large dielectric BaF_2 nanoparticles (NPs) incorporated PVDF thin film has been prepared via *in situ* process followed by solution casting procedure. We have demonstrated a more simple, cost-effective and efficient prototype Self-Charged Hybrid Photo-Power Cell (HPPC) by integrating a dye-sensitized solar light capturing and converting part with large dielectric BaF_2/PVDF thin film as storage unit in a single power pack. Our light-weighted self-charged HPPC is able to charge under visible light without any external electrical bias which may be used as power supplier unit in portable electronic gadgets.

2. Experimental

2.1. Materials

The used materials for synthesizing the BaF_2/PVDF thin films are Poly (vinylidenefluoride) (PVDF) pellets (Aldrich, Germany. M_w: 275,000 GPC, M_n: 71,000), Strontium nitrate ($Ba(NO_3)_2$) (CDH, India), Ammonium fluoride (NH_4F) (Merck, India), dimethyl sulfoxide, (DMSO) (Merck, India). For the HPPC fabrication, we have used FTO coated glass (Sigma Aldrich, Germany), Phenosafranine (PSF) (Sigma Aldrich, Germany), polyvinyl pyrrolidone (PVP) (Loba Chemie) and TiO_2 NPs (See supporting information for preparation process), Orthophosphoric acid (H_3PO_4) (Merck, India). All the materials or chemicals are purchased from the above mentioned chemical companies. The synthesis and design of BaF_2 NPs incorporated PVDF films and our device are described in Sections 2.2 and 2.3 in detail. TiO_2 NPs has been prepared in laboratory and the procedure and used chemicals are discussed in supporting information.

2.2. In situ synthesis of BaF_2 NPs incorporated PVDF films

At first, two solutions of $Ba(NO_3)_2$ and NH_4F have been separately prepared within initially produced 4% PVDF – DMSO solution at 60 °C with different molar concentration (0.01–0.2 (M)) and (0.02–0.4 (M)) respectively. Then, NH_4F/DMSO solution has been slowly poured into PVDF/$Ba(NO_3)_2$ solution and stirred continuously in magnetic stirrer at 80 °C. BaF_2 NPs have been formed within PVDF matrix after addition of NH_4F solution into the PVDF/$Ba(NO_3)_2$/DMSO mixture. Thereafter, BaF_2/PVDF NC films have been obtained by evaporating the solvent in a dust free oven at 80 °C for 12 h using solvent casting method. Simultaneously, pure PVDF film is also prepared using the same procedure in same condition. All the films have been collected in a vacuum desiccator for further characterization. The average thickness of the prepared films are 20 μm. The different concentrations of BaF_2 NPs in PVDF matrix (0.01–0.2 M) have been tabulated in Table S1 (see supporting information).

2.3. HPPC fabrication

Initially, PSF (20 mg/ml), TiO_2 NPs (100 mg/ml), H_3PO_4 and PVP (10% mass) are added to 5 ml distilled water and stirred magnetically for 6 h to prepare the light sensitive dye solution. Then, 20 μl dye solution has been casted on two unstrained FTO coated glasses and dried at 50 °C temperature. When the dye solution has become sticky, the previously prepared *in situ* PVDF/BaF_2 NCs (0.15 M) and pure PVDF thin films deposited on two aluminium foils are placed on the sticky layer of the FTOs separately. Further drying ensures the evaporation of water completely and optimize contact between the dye layer and the PVDF based films. To investigate photovoltaic phenomenon of our synthesized HPPCs, two wires are connected with the acting electrode FTO and counter Al electrode respectively (Fig. 1).

2.4. Characterization

2.4.1. X-ray diffraction (XRD)

The formation of the NPs and β phase of the pure and NC doped films have been verified by X-ray diffractometer (Model-D8, Bruker AXS Inc, Madison, WI) with scan speed of 0.3 s/step using Cu-K_α irradiation working under a voltage of 40 kV in 2θ range from 10° to 50°.

2.4.2. Fourier transform infrared spectroscopy (FTIR)

Further, the crystalline phases of the films are investigated using FTIR (FTIR-8400S, Shimadzu). The absorbance data have been collected by scanning the samples 50 times in the wavenumber range from 400 cm^{-1} to 1100 cm^{-1} with a resolution of 4 cm^{-1}. The β-phase fraction (F(β) %) of pure PVDF and NC films are calculated by using Lambert–Beer law

$$F(\beta) = \frac{A_\beta}{\left(\frac{K_\beta}{K_\alpha}\right)A_\alpha + A_\beta} \quad (1)$$

where Aα and Aβ are the absorbance at 764 cm^{-1} and 840 cm^{-1} respectively and Kβ (7.7×10^4 cm^2 mol^{-1}) and Kα (6.1×10^4 cm^2 mol^{-1}) are the absorption coefficients at the respective wavenumber [26].

2.4.3. Study of optical properties

The formation of BaF_2 NPs in PVDF matrix is also confirmed by a UV–Visible spectrometer (Lambda 25, Perkin Elmer, USA and UV-3101PC, Shimadzu) by recording the absorbance spectra of synthesized films in the range 200–450 nm. The photoluminescence characteristics have been characterized using a Cary Eclipse fluorescence spectrophotometer (Agilent Technologies) exciting the sample at wavelength, $\lambda_{ex} \sim 268$ nm.

2.4.4. Field emission scanning electron microscopy (FESEM)

The morphological structure of the pure PVDF and NC films have been examined by a field emission electron microscope (FESEM) (INSPECT F50, Netherland). First, the films are coated with gold through plasma spraying. The samples are placed within a vacuum chamber (Pressure $\sim 5 \times 10^{-3}$ Pa). Then FESEM images of the samples are captured under operating voltage of 20 kV, emission current 170 μA and with beam spot size of 3 mm.

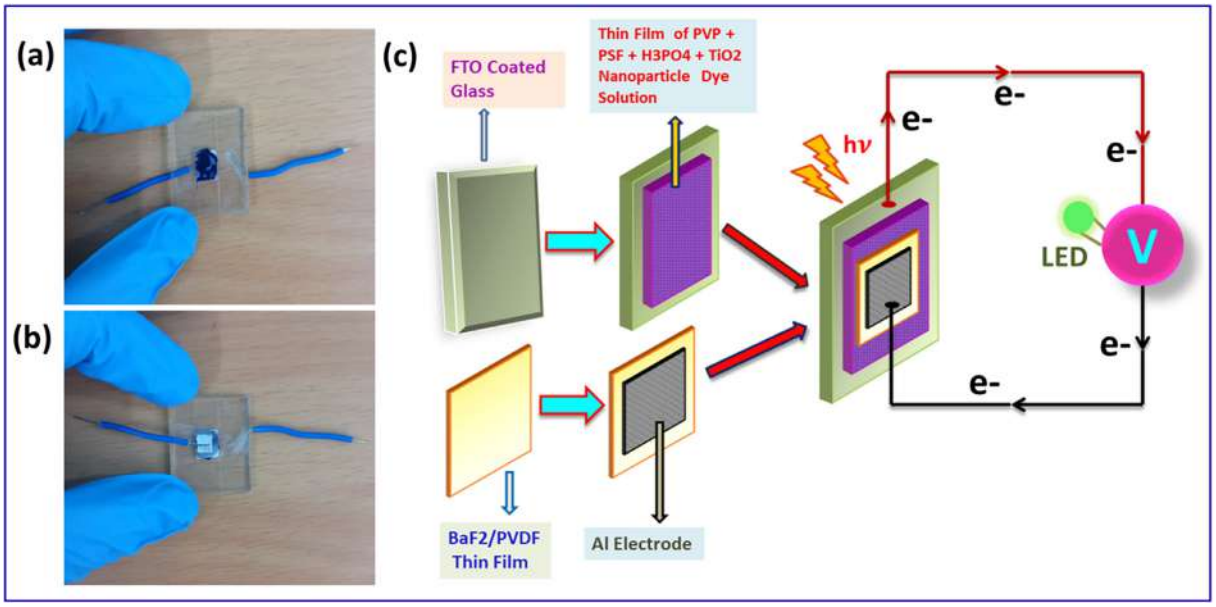

Fig. 1. (a, b) Digital image of the HPPC, (c) Schematic representation of the fabrication of the HPPC.

2.4.5. Dielectric properties measurements

The dielectric variations of the films have been studied by measuring the capacitance (C) and tangent loss (tan δ) within the frequency range 20 Hz to 2 MHz using a digital LCR meter (Agilent, E4980A) at room temperature applying 1 V ac voltage across the two opposite surfaces of the samples. The dielectric constant (ε) and the ac conductivity (σ) of the samples were calculated using the following equations,

$$\varepsilon = C.\, d/\varepsilon_0 A \tag{2}$$

$$\sigma_{ac} = 2\pi f \varepsilon_0 \varepsilon tan\delta \tag{3}$$

where d and A are the thickness and area of the samples respectively and f is the frequency in Hz applied across the samples and ε_0 is the permittivity of the free space with value 8.854×10^{-12} F m^{-1} [24,26].

2.4.6. Investigation of device performances

The output characteristics of our fabricated prototype devices are studied by connecting the two copper wires which are extended from the electrodes to a digital multi-meter (Agilent U1252A) and an electrometer (Keysight-B2985A) under light illumination and dark condition without applying any external bias voltage across the electrode of the devices.

3. Results and discussions

The digital images of the fabricated device (3 mm × 3 mm) are shown in Fig. 1a and b. The fabrication of HPPC is schematically displayed in Fig. 1c. The light absorbing part i.e. PVP-PSF-TiO_2 film deposited on FTO has been adjoined with the neighbouring energy storage part i.e. the BaF_2 NPs loaded PVDF (PBF0.15) or pure PVDF thin films casted on Al foil. The well-known TiO_2 and PSF have been used as light absorbing dyes in our present study. The novelty of present study resolves around the *in situ* synthesis and characterization of BaF_2 NPs incorporated electroactive β polymorphs rich and giant dielectric PVDF film. And to design a very simple self-charged hybrid photovoltaic power cell capable to store charge or energy in same unit effectively.

3.1. Characterization of pure PVDF and PBF NC films

3.1.1. X-ray diffraction (XRD) analysis

Fig. 2a illustrates the X-ray diffraction curves of the NPs doped PVDF and pure PVDF thin films. The existence of the strong peaks at 2θ = 19°, 22°, 31°, 36.8° and 38.6° and few weaker peaks at 2θ = 33°, 41.4°, 44.7°, 48.9°, 50.4° in the diffraction pattern of the NPs doped PVDF films confirm the formation and crystallization of the BaF_2 NPs in the polymer matrix. Existence of the non-polar α phase in pure PVDF has been confirmed by the presence of diffraction peaks at 2θ ~ 17.4° (1 0 0), 19.6° (0 2 1) and 26.3° ((2 0 1), (3 1 0)) in the XRD spectrum of pure PVDF. The characteristic peaks related to non-polar α-PVDF are completely disappeared in the NPs incorporated PVDF films [26,32–34]. Only a characteristic diffraction peak is observed strongly at 20.7° ((1 1 0), (2 0 0)) for the BaF_2/PVDF thin films confirming the electroactive β phase nucleation due to the incorporation of the NPs in PVDF matrix [35,36]. The increment of the intensity of the β-phase characteristic peak up to a certain molar concentration suggests intimate interaction of the NPs and the polymer chains due to well dissemination of the *in situ* synthesized BaF_2 NPs up to that concentration of doping (19.4 vol% loading of NPs). Further doping of the NPs leads to decrease the intensity of the β-phase characteristic peak.

Fig. 2d represents the peak intensity ratio of 20.7° and 18.3° ($I_{20.7}$/$I_{18.3}$) which is the qualitative measure of β phase content within the polymer matrix [37]. The ratio is calculated to be ~0.99 for pure PVDF. The ratio is gradually increased upto 19.4 vol% loading of NPs and then has decreased for further NPs doping concentration in PVDF. The highest value is evaluated to be 35.4 for PBF0.15 which is the clear affirmation of maximum electroactive β phase crystallization in PVDF at this concentration.

3.1.2. Fourier transform infrared (FTIR) spectroscopy

Fourier transform infrared spectroscopy (FTIR) has also been studied for investigating the phase behavior of the films shown in Fig. 2**c.** All the characteristic absorbance bands related to non-polar α phase at 489 cm^{-1} (CF2 waging), 533 cm^{-1} (CF_2 bending), 615 and 764 cm^{-1} (CF_2 bending and skeletal bending), 795 and 975 cm^{-1} (CH_2 rocking) which are present in the FTIR spectrum of pure PVDF are totally vanished in the absorbance spectra of the NPS incorporated PVDF films [23,38,39]. The absorbance band at 475 cm^{-1} (CF_2 deformation), 510 cm^{-1} (CF_2 stretching), 600 cm^{-1} (CF_2 wag) and 840 cm^{-1} (CH_2 rocking, CF_2 stretching and skeletal C–C stretching) are raised clearly indicating the nucleation of electroactive β phase within the BaF_2 NPs modified PVDF thin films [26,35]. Intensity of the mainβ phase absorbance peak at 840 cm^{-1} has been increased with the NPs

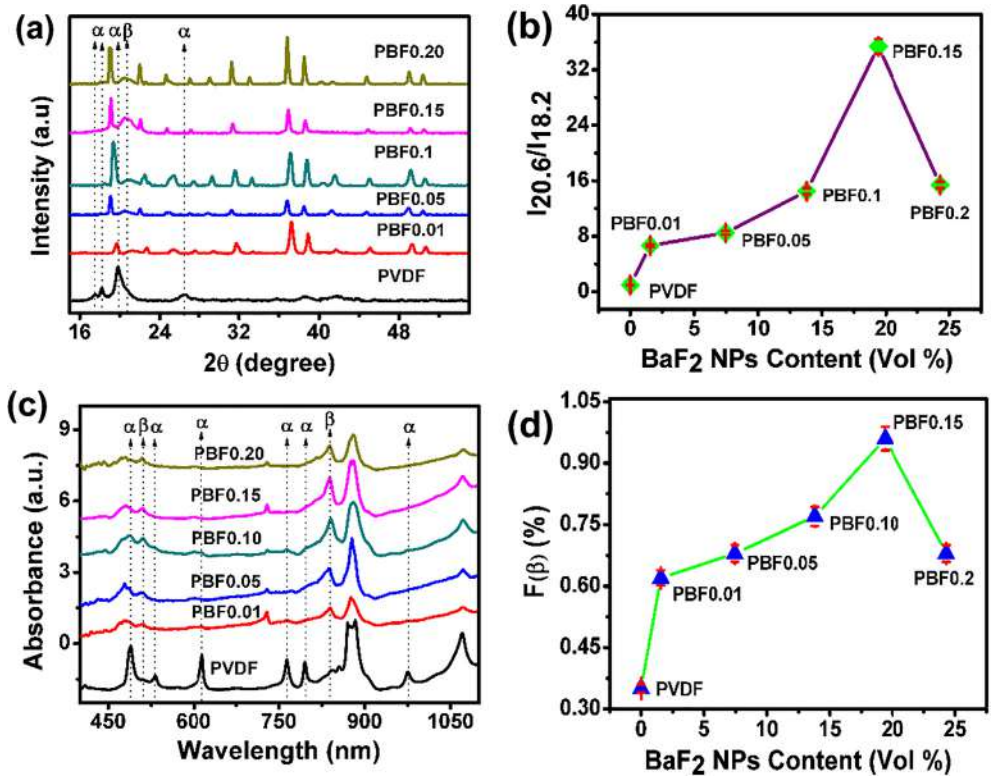

Fig. 2. (a) XRD patterns of pure PVDF and BaF_2/PVDF thin films, (b) Ratio of $I_{20.7}$ and $I_{18.3}$ of the samples. (c) FTIR spectra of pure PVDF and BaF_2/PVDF thin films, (d) β-phase content with increasing BaF_2 content form IR spectra.

concentration and becomes maximum for 19.4 vol% i.e. for PBF0.15 and decreased for the higher concentration.

The relative fraction of the β phase content i.e. F (β) (%) is evaluated using Eq. (1) and plotted against BaF_2 NPs content shown in Fig. 2d. A sharp increment of F (β) (%) with the increase of doping concentration (volume %) up to a certain value has been observed and the maximum F (β) (%) value ~96% has been obtained for PBF0.15 M. So, the FTIR data are well agreed with the XRD study. The nucleation and stabilization of electroactive β phase in BaF_2 NPs modified PVDF thin films have been accelerated by BaF_2 NPs up to a certain value due to uniform distribution and optimum electrostatic interaction between the NPs surface and the CH_2/CF_2 dipoles of the polymer chains [25,26].

3.1.3. Optical properties (UV–Visible and photoluminescence spectroscopy)

UV–Visible spectroscopy of the BaF_2/PVDF and pure PVDF thin films are depicted in Fig. 3a. For pure PVDF thin films no characteristic absorption peak has been observed. But a wide and prominent peak centred at 280 nm (~4.43 eV) has been found for the NPs loaded PVDF thin films. It signifies the formation BaF_2 NPs and the homogeneous distribution and interaction between the NPs and PVDF matrix in the BaF_2/PVDF thin films. The intensity of the absorbance peak has been raised with increasing loading concentration of the NPs suggesting the acute electrostatic interaction and uniform distribution of the NPs in polymer matrix [40]. Fig. 3b shows the photoluminescence emission spectra of the pure and NPs modified PVDF thin films. Two distinct wide emission peaks at wavelength 371 nm and 434.5 nm are appeared at excitation λ_{ex} = 268 nm. Intensity of the emission peaks are successively increased due to the more incorporation of the BaF_2 NPs in the samples. Inception of the peaks may be explained by the movement and recombination of the conduction band electrons within the different luminescence centres originated due to the internal molecular arrangement or various defects in between the NPs and polymer matrix. The absorption property of the BaF_2/PVDF films in UV region and simultaneous photoluminescence emission in both UV and visible region

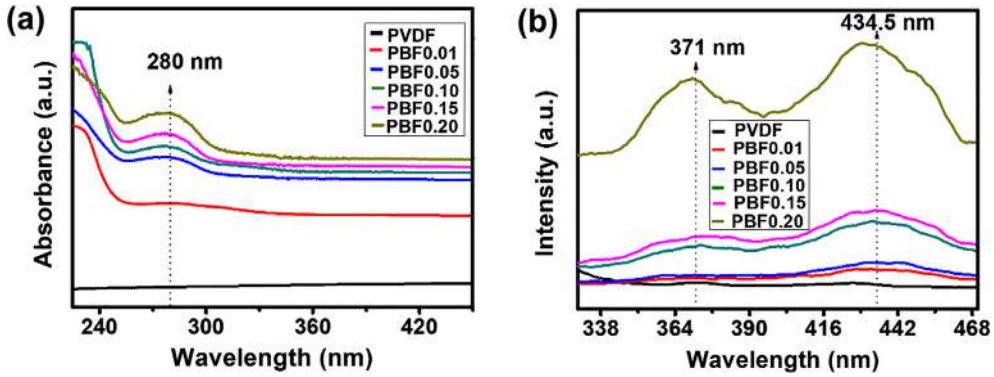

Fig. 3. (a) UV–Visible absorption spectra and (b) Photo luminescence spectra (λ_{ex} = 268 nm) of pure PVDF and BaF_2 NPs doped PVDF thin films (PBF0.01, PBF0.05, PBF0.10, PBF0.15 and PBF0.20).

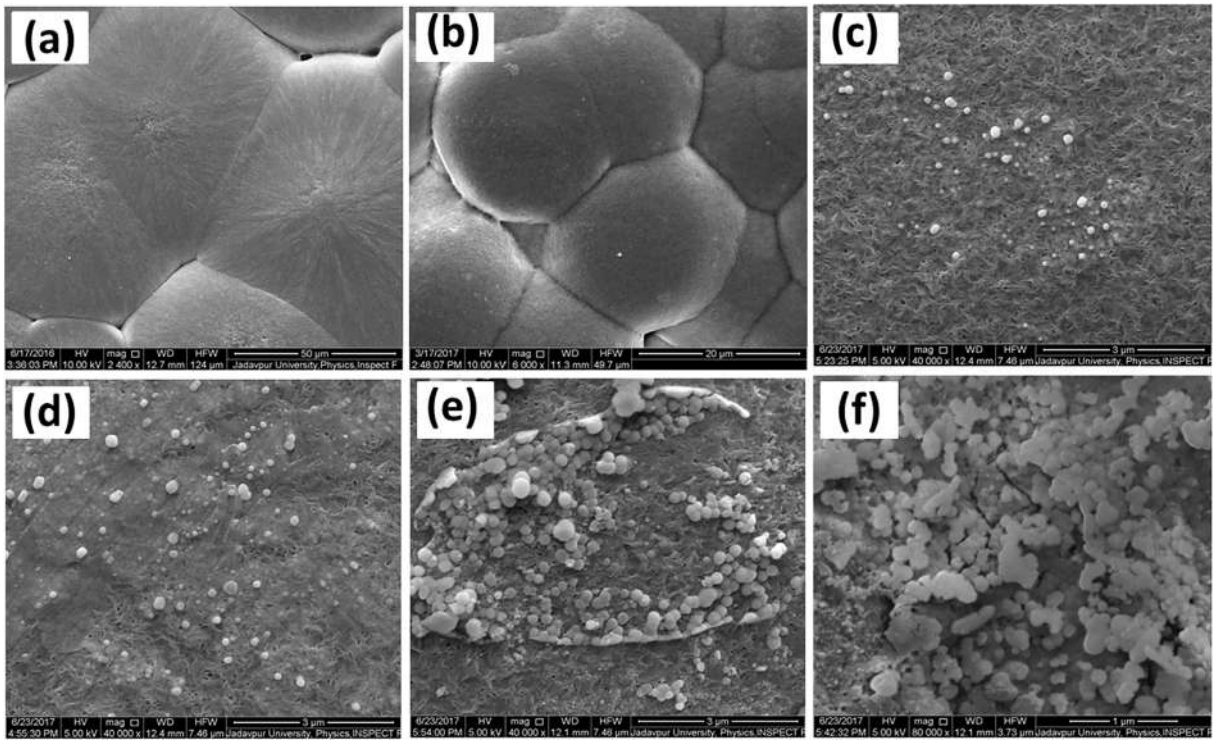

Fig. 4. FESEM images of (a) pure PVDF, (b) PBF0.01, (c) PBF0.05, (d) PBF0.10, (e) PBF0.15 and (f) PBF0.2.

is very attracting fact in the different field of application such as optoelectronics, UV protectors and sensors, and light emitting diodes (LEDs) [41].

3.1.4. Morphology and microstructure of the BaF_2 NPs modified PVDF thin films

The formation and structural morphology of the BaF_2 NPs in the polymer matrix from microscopic point of view has been studied by field emission scanning electron microscopy (FESEM). The FESEM images of the samples are shown in Fig. 4. The formation of spherical BaF_2 NPs (diameter ~ 50–80 nm) within polymer matrix has been confirmed by FESEM images of BaF_2 NPs modified PVDF thin films [42,43]. The synthesis process and the temperature are the two vital issues of controlling the size of the NPs. As the NPs are synthesized via *in situ* process in to the polymer matrix with controlled NPs grown and drying temperature, the size of the NPs is well controlled. The spherical NPs are uniformly dispersed upto 19.4 vol% loading of the NPs and agglomeration of NPs has been observed for further increase of the loading concentration of the NPs in PVDF. The formation of smaller size of the spherulites (~3 to 5 μm) due to the catalytic effect of the well distributed BaF_2 NPs suggest the nucleation of electroactive β phase in BaF_2 NPs modified PVDF thin films. While for nonpolar α polymorph, diameter of the spherulite is within 20–40 μm which is observed in pure PVDF (Fig. 4a) [44,45].

3.1.5. Dielectric properties

Fig. 5a and b illustrate the variation of the dielectric constant and tan δ with respect to BaF_2 NPs content of samples at 20 Hz and 2 MHz. The values of the dielectric constant and tan δ been increased sharply up to 19.4 vol% incorporation of BaF_2 NPs in PVDF and decreased for further loading of the NPs at 20 Hz. It is also noticeable that the values of those parameters are slowly increased at higher frequency (i.e. 2 MHz) with NPs content. The non-linear improvement of the dielectric constant at 20 Hz and a sharp increment of dielectric value at 19.4 vol% of loading of the NPs may be interpreted by the Maxwell–Wagner–Sillars (MWS) interfacial polarization [25,26,46–48]. Maximal value of the dielectric constant has been found to be ~2570 for the PBF0.15 thin film at 20 Hz frequency whereas for pure PVDF it is 9 at same frequency. Strong interconnection and well mixing of the *in situ* synthesized BaF_2 NPs with the PVDF matrix reduce the intermolecular space and enhance large number of charge carriers i.e. dipoles which have induced longer planar zigzag conformations into the polymer matrix resulting a significantly large dielectric constant of the PBF0.15 at this concentration of the NPs [26,49,50]. At lower doping of the NPs in PVDF matrix the NPs are well separated from each other and there is no possibilities of effective interaction between the NPs. When the NPs content has been increased, the interfacial area per unit volume between the polymer matrix and the NPs is increased and the inter-particle distances are reduced. Thus the average interfacial polarization has increased effectively up to the doping concentration of NPs when it has reached to percolation threshold value that is 19.4 vol%. The microstructures of the samples i.e. FESEM images also well consistent with the dielectric data. Uniform distribution of *in situ* formed NPs in polymer matrix upto the threshold value of doping also observed in FESEM image (Fig. 4) which leads to optimum interfacial surface area per unit volume of the NPs upto 19.4 vol% of NPs which effectively enhance the associated interfacial polarization by forming maximum number of micro-capacitive grains centring every NPs [24]. The agglomeration of the NPs in PBF0.20 has reduced the interfacial surface area per unit volume resulting lower dielectric value (Fig. 4f) [24,26]. The dependence of ac conductivities of the samples with NPs loading concentrations at 20 Hz and 2 MHz have been illustrated in Fig. 5c. A linear increase in ac conductivity with increment of the volume content of BaF_2 NPs is observed for both higher and lower frequencies (20 Hz and 2 MHz) with maximum values for PBF0.15. The ac conductivity values are reduced for higher loading of NPs.

Fig. 5d and e represent the frequency dependent dielectric constant and tangent loss of the pure PVDF and BaF_2 NPs modified PVDF thin films at ambient condition. The dielectric values for all samples are gradual reduced with increasing frequency as noticed (Fig. 5d**).** This decreasing phenomenon of dielectric constant may be elucidated by MWS interfacial polarization principle. Intimate interaction has been

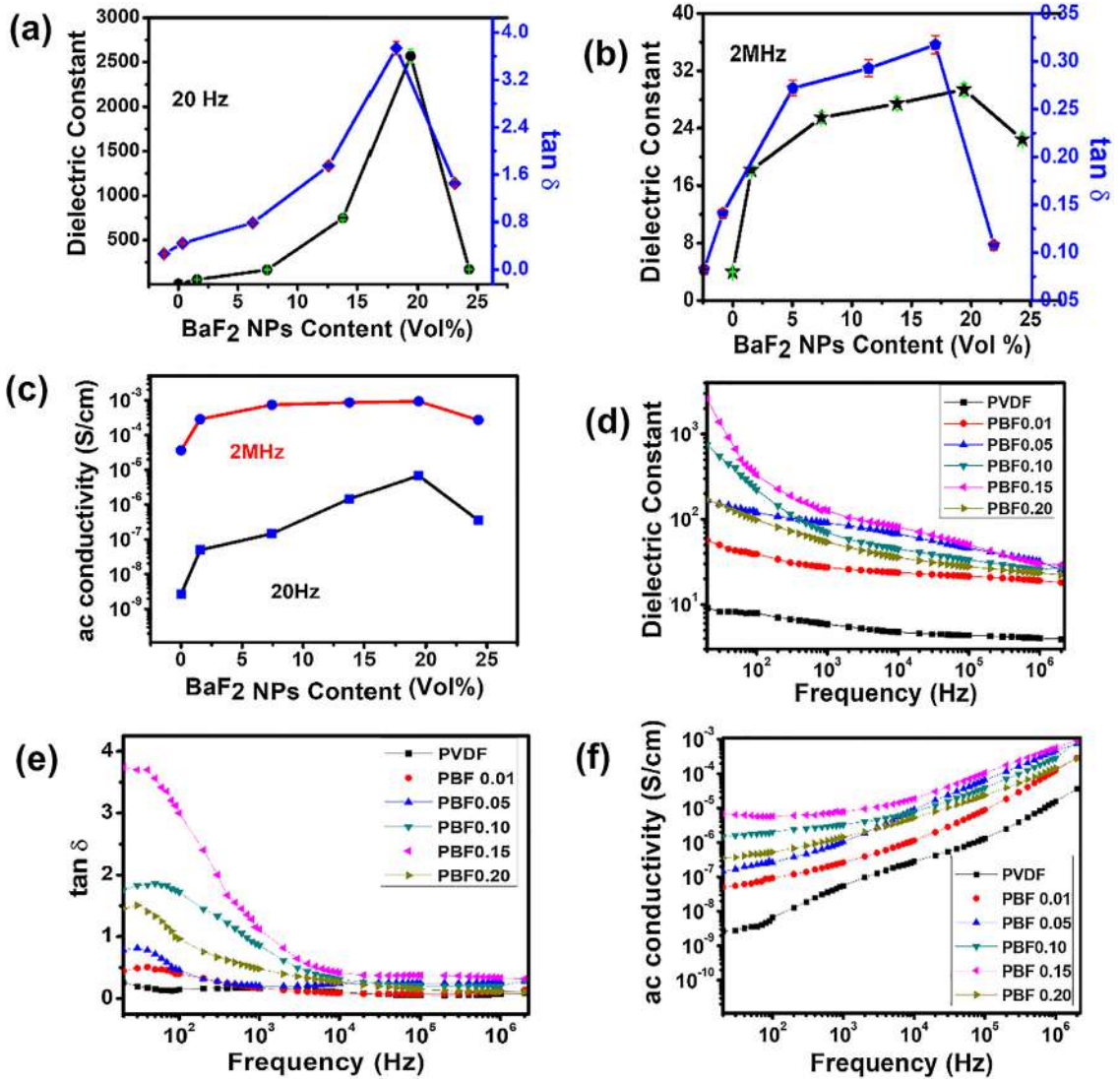

Fig. 5. BaF_2 NPs content (volume %) dependency of (a) dielectric constant, (b) tangent loss and (c) ac conductivity at 20 Hz and 2 MHz of pure and NPs incorporated PVDF thin films. Frequency dependency of (c) dielectric constant, (d) tangent loss and (e) ac conductivities of pure PVDF and NC samples.

occurred between the NPs and the PVDF chain during the ***in situ*** formation of the BaF_2 NPs within polymer matrix [46–48,51]. Thus, short range dipolar interaction and large accumulation of the space charges have arised at the interfaces of NPs and PVDF chains which develop a quite large dielectric constant at lower frequency region [36,42]. With increasing frequency, the movement and realignment process of the dipoles have been restricted and the dipoles within the polymer samples cannot follow the fast change of the frequency of the applied electric field [52]. As a result small number of dipoles are able to rearrange them with the external field which reduce the overall polarization in higher frequency region. Therefore, dielectric value is decreased with increasing frequency (Fig. 5d) [37,47,48]. The tangent loss peaks are observed for the NPs modified thin films at lower frequency region (Fig. 5d). The origination of these Debye-type dielectric relaxation peaks are mainly appeared because of the resonance or heat energy dissipation due to oscillation of the dipoles [51,53]. The ac conductivities of pure PVDF and BaF_2 NPs modified PVDF thin film are increased linearly with increasing frequency shown in Fig. 5f. The conductivity at higher frequency region is mainly regulated by the ac conductivity but the dc conductivity occurs at low frequency region. The raise of ac conductivity is mainly due the hopping of the dipoles in a definite arrangement [37,50].

3.2. Output characteristics and working mechanism of the HPPC

The photovoltaic phenomenon i.e. the self-charging and discharging behavior of the fabricated HPPCs are shown in Fig. 6. The device has been charged under visible light illumination by a 40 W tungsten bulb covered with ultra-violet and infrared light eliminator filters with intensity 110 mW/cm^2, without using any external bias voltage. According to our aforementioned studies, PBF0.15 M has come out as the most appropriate material for constructing the device. PBF0.15 thin film (thickness ~20 μm and dimension ~0.3 cm × 0.3 cm) is the most suitable charge storing material for designing the HPPC due to its large dielectric value (~2570) which has been achieved by proper incorporation of well controlled smaller sized BaF_2 NPs in PVDF matrix via *in situ* process. A composite film of TiO_2 NPs, PSF, PVP and H_3PO_4 has been used to generate photoelectrons. The dye film deposited on a FTO coated glass has been attached with the high dielectric PBF0.15 or pure PVDF thin film which are previously casted on aluminium foil. We have constructed two prototype HPPC separately by using pure PVDF and BaF_2 NPs incorporated (19.4 vol%) PVDF thin films as storing unit for comparison purpose. The HPPC fabricated using PBF0.15 is charged up to 1.3 V within 65 s under the visible light illumination (~110 mW/cm^2) whereas the maximum voltage is obtained ~0.87 V within 95 s for the device constructed with pure PVDF film shown in Fig. 6c and d

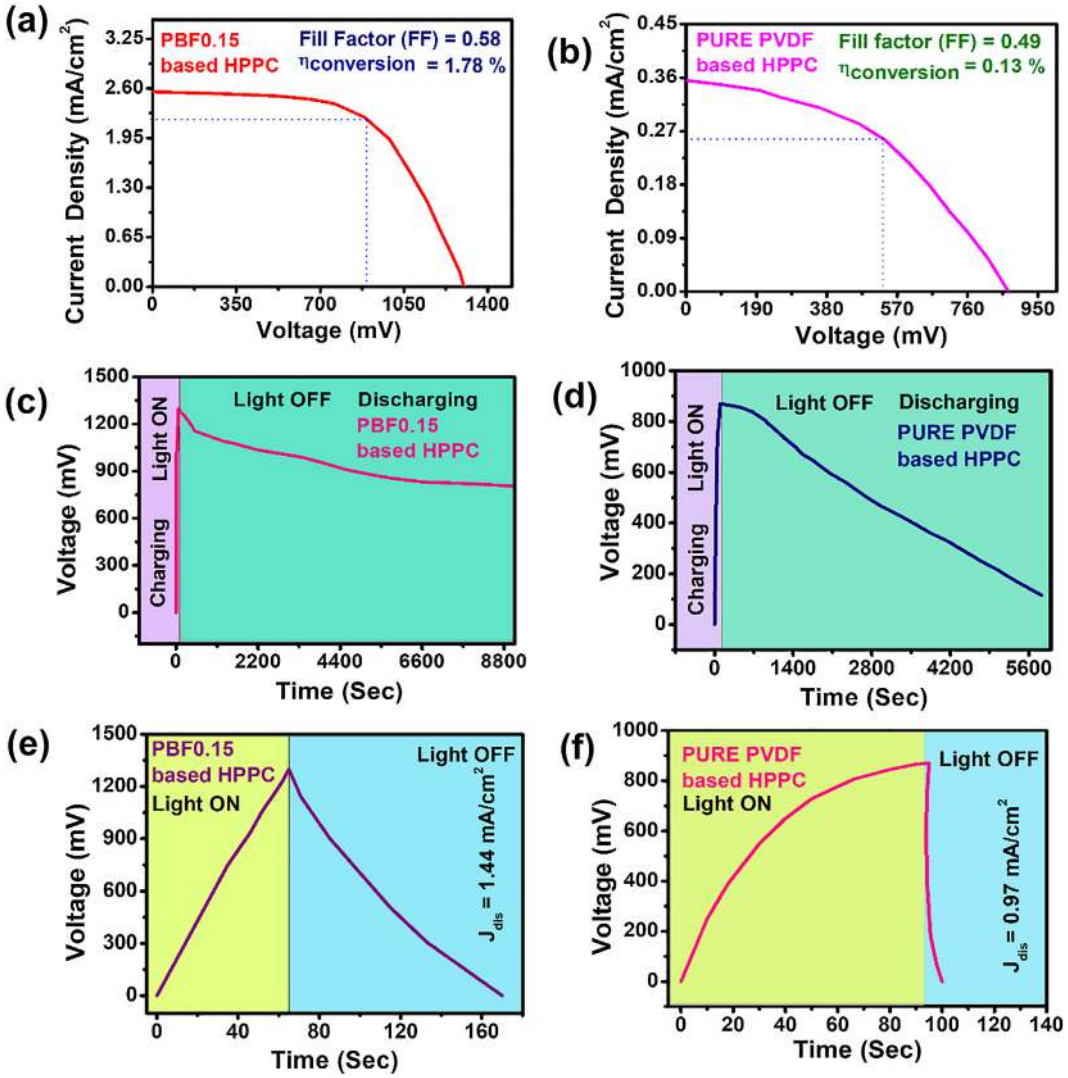

Fig. 6. (a, b) J-V curve and (c, d, e, f) Self-charging and discharging voltage–time (V-t) curves of HPPC fabricated by PBF0.15 and pure PVDF film.

respectively. The current density (J)-open circuit voltage characteristics of the HPPC with PBF0.15 and pure PVDF thin film are illustrated in Fig. 6a and b respectively. The short circuit current density (J_{sc}) is found to be ~2.6 mA/cm^2 and 0.3 mA/cm^2 for the PBF0.15 and pure PVDF film based HPPC respectively.

The photoelectrons have been generated by the solar part i.e., composite dye film of TiO_2, PSF, PVP and H_3PO_4. Under light illumination the dye film is excited and the electrons are jumps to its conduction band or LUMO by absorbing photons ($h\nu$). The UV–Vis absorption spectroscopy and the HOMO-LUMO states of the composite dye film are schematically shown in Fig. 7a. According to the anatomy of the energy diagram, photoelectrons generated by PSF molecules by absorbing the light (LUMO ~ −3.07 eV) are injected to the lowest energy level of conducting FTO (−4.4 eV) through TiO_2 NPs (LUMO ~ −4.21 eV). Here, The main function of TiO_2 NPs is to restrict the electron-hole recombination by conducting the photoelectrons generated by PSF towards the FTO and this fact has improved the performance of our HPPC [54,55]. The photoelectrons are injected to FTO have immediately travelled towards the Al electrode through the connected Cu wire [8,56].

As the high dielectric PBF0.15 thin film has placed in between the solar part and Al electrode, the photoelectrons have been stored between the junction of Al and PBF0.15 as well as the interfaces of the BaF_2 NPs and the polymer matrix resulting a voltage generation in our HPPC. The insufficiency of electrons of PSF molecules are fulfilled by the donation of electrons from PVP and H_3PO_4. This electron generation process has been repeated and counter electrode (Al) terminal has charged negatively by accumulating and storing the photoelectrons in the PBF0.15 by forming large number of micro-capacitor type structures around the BaF_2 NPs in PBF0.15. The presence of BaF_2 NPs in PVDF matrix has effectively enhanced the charge storage capability of PBF0.15 by improving its dielectric value (~2570) which is also previously confirmed in dielectric properties section. At the same time, the solar part becomes positively charged due to generation holes. Thus, a potential difference has existed between the electrodes which results a large open circuit voltage 1.3 V under fully charged condition of PBF0.15 based HPPC [8,57]. Under fully charged condition the photoelectrons generation process has been completely ceased and the J_{sc} become zero [22,23,58]. The photoelectrons formation and recombination process by absorbing visible photons from light irradiation are as follows:

$$PSF + h\nu = PSF^+ + e^-,\ PVP \rightarrow PVP^-,\ PSF^+ + PVP^- = PSF + PVP^+$$

$$H_3PO_4 \rightarrow H_3PO_4{}^-,\ PSF^+ + H_3PO_4 = PSF + H_3PO_4{}^*$$

After completion of the charging process the light is switched off and the charge storage stability of our devices have been tested in dark atmosphere. Initially, a very small fall in voltage is observed for

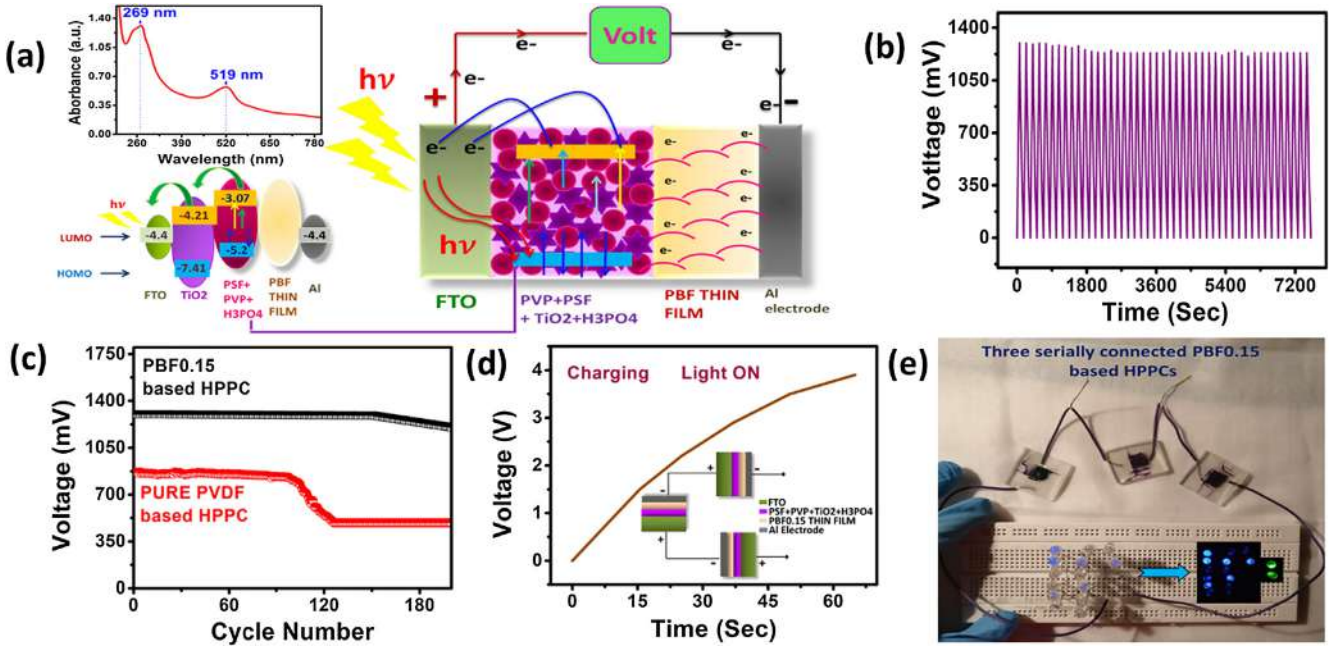

Fig. 7. (a) UV–Visible absorption spectrum of the dye film, schematic presentation of HOMO-LUMO energy states and the probable photoelectrons generation and storage mechanism. (b, c) Investigation of self-charging and discharging recyclability or durability test ((a) charge/discharge V-t profile for 45 days (1 cycle per day) and (c) recycling test for 200 cycles of the PBF0.15 based HPPC under light and dark ambient. (d) V-t curve of three PBF0.15 based HPPCs connected in series under light illumination. (e) Digital image of glowing of the 14 blue and 2 green LEDs by serially connected three PBF0.15 based HPPCs as a power pack. (For interpretation of the references to colour in this figure legend, the reader is referred to the web version of this article.)

PBF0.15 based HPPC and the voltage becomes almost constant for long time indicating the charge storage ability and low internal recombination of electrons and holes (shown in Fig. 6c). For the pure PVDF based HPPC the output voltage reaches to its initial value within 96 min (approximately) (Fig. 6d). The storing ability and slow internal electrons-holes recombination in fully charged PBF0.15 based HPPC are mainly due to the dissimilarity of the dielectric value of PBF0.15 (~2570 that is 200 times greater than pure PVDF) and the formation of many micro-capacitors in the BaF_2 NPs incorporated PVDF film i.e. PBF0.15 sample. The PBF0.15 based HPPC and pure PVDF based HPPC have been discharged with a constant discharge current density ~1.44 mA/cm^2 and ~0.97 mA/cm^2 respectively. The output voltage has been discharged to its initial value within 105 s for PBF0.15 based HPPC and 5 s for the pure PVDF based device (Fig. 6e and f). The output characteristics i.e. stored charge, capacitance, energy density and power density of our two prototype HPPCs have been evaluated from the discharge curves (Fig. 6e and f) by the following equations:

$$Q = \int J_{dis} dt \tag{4}$$

$$C = Q/dV \tag{5}$$

$$E_{output} = 1/2CV^2 \tag{6}$$

$$P = VJ_{dis} \tag{7}$$

where Q, C, E_{output}, P, J_{dis}, dt and dV are the charge density, capacitance, output energy density, power density, discharge current density, discharge time and voltage difference respectively. Maximum energy density is calculated to be ~281.6 mWh/m^2 with excellent power density ~18.7 W/m^2 and specific areal capacitance 1200 F/m^2 for HPPC fabricated by PBF0.15. Whereas for pure PVDF based HPPC, the value of energy density, power density and specific areal capacitance are evaluated to be ~5.9 mWh/m^2, 8.4 W/m^2 and 55.7 F/m^2 respectively (See comparison Table S2 supplied as supporting information).

Further the fill factors (FF) from J-V curve and the energy conversion efficiency of our HPPCs (Fig. 6a and b) are calculated by using the Eqs. (8) and (9)

$$FF = \frac{V_{pp} \times I_{PP}}{V_{OC} \times I_{SCl}} \tag{8}$$

$$\eta_{conversion}\% = \frac{P_{out}}{P_{in}} \times 100 = \frac{v_{OC} \times I_{SC} \times FF}{P_{in}} \times 100 \tag{9}$$

where v_{OC} = open circuit voltage, I_{SC} = short circuit current, FF = fill factor, P_{in} = the incident light power = 110 mW/cm^2, V_{pp} = voltage power point, I_{PP} = current power point, (Here I_{SC} and I_{PP} are in mA/cm^2, v_{OC} and V_{pp} are in mV, P_{in} and P_{out} are in mW).

By using Eqs. (6) and (9) and the following equations the overall and storage efficiencies of our fabricated devices are evaluated. A summarized output characteristic values for our both devices are tabulated in Table 1.

$$\text{Overall efficiency, } \eta_{overall}\% = \frac{E_{output}}{E_{input}} \times 100 \tag{10}$$

$$\eta_{storage} = \frac{\eta_{overall}\%}{\eta_{conversion\%}} \tag{11}$$

where the input energy density $E_{input} = P_{in} \times dt'$ and dt' is the charging time [59].

The values of efficiency parameters for the PBF0.15 based HPPC are considerably higher than that of the pure PVDF based HPPC. The novelty of our integrated PBF0.15 based HPPC is not only circulate around

Table 1
Summarized of the output characteristics of the HPPC (See comparison Table S2 supplied as supporting information).

Parameters	PBF0.15 based HPPC	Pure PVDF based HPPC
Energy density	281.6 mWh/m^2	5.9 mWh/m^2
Power density	18.7 W/m^2	8.4 W/m^2
Storage ability	1200 F/m^2	55.7 F/m^2
Energy conversion Efficiency	1.78%	0.125%
Energy storage efficiency	79%	16%
Overall efficiency	1.41%	0.02%

the high photovoltage generation, but also around the efficient conversion and storage of energy for a long time which are the basic criteria of a device for practical utility.

The longevity or durability of our PBF0.15 based device has examined by recording the data of photovoltaic performance i.e. self-charging and discharging variation for 45 days (1 cycle per day) and testing the charge-discharge profiles for 200 cycles (Fig. 7b and c). The durability i.e. recycling performances of pure PVDF based HPPC is tested and shown in Fig. 7c. The generation of photovoltage by the PBF0.15 based HPCC is decreased only by 5.2% after 200 cycles. Whereas, the photovoltage generation of pure PVDF based HPPC has considerably dropped to its half value within 90 cycles (Fig. 7c). The practical utilization of our PBF0.15 based HPPC has been demonstrated by glowing commercially available light emitting diodes of two colours using three serially connected device as power pack. The self-charging characteristic i.e. V-t curve of our hybrid device under light is graphically shown in Fig. 7d. The combined devices are charged up to 3.9 V within 65 s which is able to lightening up 14 blue and 2 green LEDs with high intensity for long time (7 days). The digital snapshot of glowing of LEDs by three serially connected PBF0.15 based HPPC are shown in Fig. 7e. A video of the whole circuit connection of the PBF0.15 based HPPC with demonstration of glowing of LEDs is supplied as supporting data (Video-S1 and Video S2). Our simplistic approach to design the hybrid self-charged photo-power cell with very good energy storage ability may have a promising impact in the field clean energy harvesting and storing fields. But, the overall and solar energy conversion efficiencies are still low. This shortcomings of our prototype device may be further enhanced by focussing on proper choice and optimization of solar light sensitive materials (like ZnO, CdS, etc.) to improve the conversion solar energy. In future, our study will be focused to enhance the overall and conversion efficiency by choosing some efficient new dyes and NPs.

4. Conclusions

Thus, we have successfully synthesized electroactive and giant dielectric BaF_2 NPs incorporated PVDF thin film via *in situ* grown of the NPs followed by solution casting process. Uniform distribution and strong interfacial interaction between the NPs and the polymer chains in the NCs have improved the electroactive β phase nucleation ~ 96% and the dielectric constant ~2570 at 20 Hz for 19.4 vol% incorporation of the NPs. Thereafter we have designed an inexpensive and highly efficient prototype hybrid photo-power cell i.e. HPPC for converting the solar energy to electrical energy with superior energy storage function in same unit. Very popular PSF and TiO_2 NPs have been used as solar energy absorbing and conversion unit which has been successfully adjoined with our developed high dielectric PBF0.15 thin film acting as the storage unit of the photogenerated electrons. Maximum energy storage efficiency ~79% is obtained for our PBF0.15 based HPPC that is much greater than the storage efficiency of pure PVDF based HPPC (~16%). The energy storage stability and the practical utilization of our HPPC is evidently verified by glowing up 14 blue LEDs and 2 green LEDs for 7 days. Our prototype HPPC may have the potential to fulfil the recent power hunger of portable electronic tools as well as our modern society.

Acknowledgement

Authors are grateful to Department of Higher Education, Science & Technology and Biotechnology, Government of West Bengal, India and University Grants Commission (UGC), India for financial assistance.

Appendix A. Supplementary material

Supplementary data associated with this article can be found, in the online version, at https://doi.org/10.1016/j.enconman.2018.06.050.

References

[1] Liu C, Li F, Ma L-P, Cheng H-M. Advanced materials for energy storage. Adv Mater 2010;22:28–62.
[2] Genwa KR, Sagar CP. Energy efficiency, solar energy conversion and storage in photogalvanic cell. Energy Convers Manage 2013;66:121–6.
[3] Kousksouan T, Bruelb P, Jamilc A, El Rha fikid T, Zeraoulia Y. Energy storage: applications and challenges. Sol Energy Mater Sol Cells 2014;120:59–80.
[4] Thavasi V, Singh G, Ramakrishna S. Electrospun nanofibers in energy and environmental applications. Energy Environ Sci 2008;1:205–21.
[5] Vieira FM, Moura PS, de Almeida AT. Energy storage system for self-consumption of photovoltaic energy in residential zero energy buildings. Renew Energy 2017;103:308–20.
[6] Li X, Zhang H, Mai Z, Zhang H, Vankelecom I. Ion exchange membranes for vanadium redox flow battery (VRB) applications. Energy Environ Sci 2011;4:1147–60.
[7] Gupta R, Sharma NK, Tiwari P, Gupta A, Nigam N, Gupta A. Application of energy storage devices in power systems. Int J Eng Sci Technol 2011;3:289–97.
[8] Xu J, Chen Y, Dai L. Efficiently photo-charging lithium-ion battery by perovskite solar cell. Nat Commun 2015;6:1–7.
[9] Zi Y, Wang ZL. Nanogenerators: an emerging technology towards nanoenergy. Appl Mater 2017;5:074103-1–074103-12.
[10] Zhang J-J, Wei Z, Huang T, Li Z-L, Yu A-S. Carbon coated TiO_2–SiO_2 nanocomposites with highgrain boundary density as anode materials for lithium-ion batteries. J Mater Chem A 2013;1:7360–9.
[11] Zhang Q, Dandeneau CS, Zhou X, Cao G. ZnO nanostructures for dye-sensitized solar cells. Adv Mater 2009;21:4087–108.
[12] Kwon J, Jilm M, Kim CU, Won SH, Kang SB, Kang SH, et al. Two-terminal DSSC/silicon tandem solar cells exceeding 18% efficiency. Energy Environ Sci 2016;9:3657–65.
[13] Lee Michael M, Teuscher J, Miyasaka T, Murakami TN, Snaith HJ. Efficient hybrid solar cells based on meso-superstructured organometal halide perovskites. Science 2012. http://dx.doi.org/10.1126/ 1228604:1-5.
[14] Murakami TN, Kawashima N, Miyasaka T. A high-voltage dye-sensitized photocapacitor of a three-electrode system. Chem Commun 2005;26:3346–8.
[15] Zhang X, Huang X, Li C, Jiang H. Dye-sensitized solar cell with energy storage function through PVDF/ZnO nanocomposite counter electrode. Adv Mater 2013;25:4093–6.
[16] Wee G, Salim T, Lam Y-M, Mhaisalkarab S-G, Srinivasan M. Printable photo-supercapacitor using single-walled carbon nanotubes. Energy Environ Sci. 2011;4:413–6.
[17] Chen T, Qiu L, Yang Z, Cai Z, Ren J, Li H, et al. An integrated "energy wire" for both photoelectric conversion and energy storage. Angew Chem 2012;51:11977–80.
[18] Wang Q, Chen H, McFarland E, Wang L. Solar rechargeable batteries based on lead-organohalide electrolyte. Adv Energy Mater 2015;5:1–6.
[19] Chien CT, Hiralal P, Wang DY, Huang I, Chen CC, Chen CW, et al. Graphene-based integrated photovoltaic energy harvesting/storage device. Small 2015;11:2929–37.
[20] Zhou F, Ren Z, Zhao Y, Shen Xinpeng, Wang Aiwu, Li YY, et al. Perovskite photovoltachromic supercapacitor with all-transparent electrodes. ACS Nano 2016;10:5900–8.
[21] Zhang M, Zhou QQ, Chen J, Yu XW, Huang L, Li YR, et al. An ultrahigh-rate electrochemical capacitor based on solution-processed highly conductive PEDOT:PSS films for AC line-filtering. Energy Environ Sci 2016;9:2005–10.
[22] Khatun F, Hoque NA, Thakur P, Sepay N, Roy S, Bagchi B, et al. 4̂-Chlorochalcone assisted electroactive β polymorph rich and high dielectric PVDF film based simplex and talented energy storage system capable of self-charging under light. Energy Technol 2017;5:2205–15.
[23] Roy S, Thakur P, Hoque NA, Bagchi B, Sepay N, Khatun F, et al. Electroactive and high dielectric folic acid/PVDF composite film rooted simplistic organic photovoltaic self-charging energy storage cell with superior energy density and storage capability. Appl Mater Interfaces 2017;9:24198–209.
[24] Thakur P, Kool A, Hoque NA, Bagchi B, Khatun F, Biswas P, et al. Superior performances of in situ synthesized ZnO/PVDF thin film based selfpoled piezoelectric nanogenerator and self-charged photo-power bank with high durability. Nano Energy 2018;44:456–67.
[25] Hoque NA, Thakur P, Roy S, Kool A, Bagchi B, Biswas P, et al. Er^{3+}/Fe^{3+} stimulated electroactive, visible light emitting, and high dielectric flexible PVDF film based PENGs: a simple and superior self-powered energy harvester with remarkable power density. ACS Appl Mater Interfaces 2017;9:23048–59.
[26] Thakur P, Kool A, Bagchi B, Das S, Nandy P. Effect of in situ synthesized Fe_2O_3 and Co_3O_4 nanoparticles on electroactive β phase crystallization and dielectric properties of poly(vinylidene fluoride) thin films. Phys Chem Chem Phys 2015;17:1368–78.
[27] Wang G. Enhanced dielectric properties of three-phase-percolative composites based on thermoplastic-ceramic matrix ($BaTiO_3$ + PVDF) and ZnO radial nanostructures. ACS Appl Mater Interfaces 2010;2:1290–3.
[28] Wang ZL, Song J. PENGs based on zinc oxide nanowire arrays. Science 2006;14:242–6.
[29] Khan U, Hinchet R, Ryu H, Kima S-W. Research update: nanogenerators for self-powered autonomous wireless sensors. Appl Mater 2017;5:073803-4–073803-13.
[30] Martins P, Costa CM, Ferreira JCC, Lanceros-Mendez S. Correlation between crystallization kinetics and electroactive polymer phase nucleation in ferrite/poly(vinylidene fluoride) magnetoelectric nanocomposites. J Phys Chem B 2012;116:794–801.
[31] Jia N, Xing Q, Liu X, Sun J, Xia G, Huang W, et al. Enhanced electroactive and mechanical properties of poly(vinylidene fluoride) by controlling crystallization

and interfacial interactions with low loading polydopamine coated $BaTiO_3$. J Colloid Interface Sci 2015;453:169–76.
[32] Achabya MEL, Arrakhiz FZ, Vaudreuil S, Essassi EM, Qaiss A. Piezoelectric -polymorph formation and properties enhancement in grapheme oxide – PVDF nanocomposite films. Appl Surface Sci 2012;258:7668–77.
[33] Martins P, Costa CM, Lanceros-Mendez S. Nucleation of electroactive β-phase poly (vinilidene fluoride) with $CoFe_2O_4$ and $NeFe_2O_4$ nanofillers: a new method for the preparation of multiferroic nanocomposites. Appl Phys A 2011;103:233–7.
[34] Mandal BP, Vasundhara K, Abdelhamid E, Lawes G, Salunke HG, Tyagi AK. Improvement of magnetodielectric coupling by surface functionalization of nickel nanoparticles in Ni and polyvinylidene fluoride nanohybrides. J Phys Chem C 2014;118:20819–25.
[35] Martins P, Lopes AC, Lanceros-Mendez S. Electroactive phases of poly(vinylidene fluoride): determination, processing and applications. Prog Polym Sci 2014;39:683–706.
[36] Thakur P, Kool A, Bagchi B, Hoque NA, Das S, Nandy P. In situ synthesis of $Ni(OH)_2$ nanobelt modified electroactive poly(vinylidene fluoride) thin films: remarkable improvement in dielectric properties. Phys Chem Chem Phys 2015;17:13082–91.
[37] Thakur P, Kool A, Bagchi B, Das S, Nandy P. Enhancement of β phase crystallization and dielectric behavior of kaolinite/halloysite modified poly(vinylidene fluoride) thin films. Appl Clay Sci 2014;99:149–59.
[38] Gonçalves R, Martins PM, Caparrós C, Martins P, Benelmekki M, Botelho G, et al. Nucleation of the electroactive β-phase, dielectric and magnetic response of poly (vinylidene fluoride) composites with Fe_2O_3 nanoparticles. J Non-Cryst Solids 2013;361:93–9.
[39] Ribeiro C, Sencadas V, Gómez Ribelles JL, Lanceros-Méndez S. Influence of processing conditions on polymorphism and nanofiber morphology of electroactive poly(vinylidene fluoride) electrospun membranes. Soft Mater 2010. 10.1080:1-25.
[40] Grass RN, Stark JW. Flame synthesis of calcium-, strontium-, barium fluoride nanoparticles and sodium chloride. Chem Commun 2005;1767:1767–9.
[41] Müller V, Rasp M, Rathouský J, Schütz B, Niederberger M, Fattakhova-Rohlfing D. Transparent conducting films of antimony-doped tin oxide with uniform mesostructure assembled from preformed nanocrystals. Small 2010;6:633–7.
[42] Mandal D, Kim KJ, Lee JS. Simple synthesis of palladium nanoparticles, β-phase formation, and the control of chain and dipole orientations in palladium-doped poly (vinylidene fluoride) thin films. Langmuir 2012;28:10310–7.
[43] Seyhan Ince-Gunduz B, Alpern R, Amare D, Crawford J, Dolan B, Jones S, et al. Impact of nanosilicates on poly(vinylidene fluoride) crystal polymorphism: Part 1. Melt-crystallization at high supercooling. Polymer 2010;51:1485–93.
[44] Thakur P, Kool A, Bagchi B, Hoque NA, Das S, Nandy P. The role of cerium(III)/yttrium(III) nitrate hexahydrate salts on electroacntive b phase nucleation and dielectric properties of poly(vinylidene fluoride) thin films. RSC Adv 2015;5:28487–96.
[45] Mandal D, Henkel K, Schmeißer D. The electroactive β-phase formation in poly (vinylidene fluoride) by gold nanoparticles doping. Mater Lett 2012;73:23–125.
[46] Tang C-W, Li B, Sun L, Lively B, Zhong W-H. The effects of nanofillers, stretching and recrystallization on microstructure, phase transformation and dielectric properties in PVDF nanocomposites. Eur Polym J 2012;48:1062–72.
[47] Li Y, Huang X, Hu Z, Jiang P, Li S, Tanaka T. Large dielectric constant and high thermal conductivity in poly(vinylidene fluoride)/barium titanate/silicon carbide three-phase nanocomposites. ACS Appl Mater Interfaces 2011;3:4396–403.
[48] Wu W, Huang X, Li S, Jiang P, Toshikatsu T. Novel three-dimensional zinc oxide superstructures for high dielectric constant polymer composites capable of withstanding high electric field. J Phys Chem C 2012;116:24887–95.
[49] Lopes AC, Silva PM, alves RG, Pereira MFR, Botelho G, Fonseca AM, et al. Enhancement of the dielectric constant and thermal properties of r-poly(vinylidene fluoride)/zeolite nanocomposites. J Phys Chem C 2010;114:14446–52.
[50] Firmino Mendes S, Costa CM, Sencadas V, Serrado Nunes J, Costa P, Gregorio Jr R, et al. Effect of the ceramic grain size and concentration on the dynamical mechanical and dielectric behaviour of poly(vinilidene fluoride)/$Pb(Zr_{0.53}Ti_{0.47})O_3$ composites. Appl Phys A 2009;96:899–908.
[51] Zhang Z, Gu Y, Wang S, Li M, Bi J, Zhang Z. Enhancement of dielectric and electrical properties in BT/SiC/PVDF three-phase composite through microstructure tailoring. Composites: Part A 2015;74:88–95.
[52] Zhou W, Zhao KS. The study of dielectric properties of 4A zeolites dispersed in silicone oil. Colloids Surfaces A: Physicochem Eng Aspects 2008;317:10–6.
[53] Lopes AC, Costa CM, Serra RSi, Neves IC, Ribelles JLG, Lanceros-Méndez S. Dielectric relaxation, AC conductivity and electric modulus in poly(vinylidene fluoride)/NaY zeolite composites. Solid State Ionics 2013;235:42–50.
[54] Hou K, Tian B, Li F, Bian Z, Zhao D, Huang C. Highly crystallized mesoporous TiO_2 films and their applications in dye sensitized solar cells. J Mater Chem 2005;15:2414–20.
[55] Mohapatra K, Kondamudi SN, Banerjee S, Misra M. Functionalization of self-organized TiO_2 nanotubes with Pd nanoparticles for photocatalytic decomposition of dyes under solar light illumination. Langmuir 2008;24:11276–81.
[56] Xu J, Wu H, Lu L, Leung S-F, Chen D, Chen X, et al. Integrated photo-supercapacitor based on Bi-polar TiO_2 nanotube arrays with selective one-side plasma-assisted hydrogenation. Adv Funct Mater 2014;24:1840–6.
[57] Liu Z, Zhong Y, Sun B, Liu X, Han J, Shi T, et al. Novel integration of perovskite solar cell and supercapacitor based on carbon electrode for hybridizing energy conversion and storage. ACS Appl Mater Interfaces 2017;9:22361–8.
[58] Hao S, Wu J, Fan L, Huang Y, Lin J, Wei Y. The influence of acid treatment of TiO_2 porous film electrode on photoelectric performance of dye-sensitized solar cell. Sol Energy 2004;76:745–50.
[59] Fu Y, Wu H, Ye S, Cai X, Yu X, Hou S, et al. Integrated power fiber for energy conversion and storage. Energy Environ Sci 2013;6:805–12.